

Barycentric Interpolation Based on Equilibrium Logarithmic Potential

Kelong Zhao¹ and Shuhuang Xiang^{2*}

¹School of Mathematics and Statistics, Central South University,
Changsha, 410083, Hunan, People's Republic of China.

²School of Mathematics and Statistics, Central South University,
Changsha, 410083, Hunan, People's Republic of China.

*Corresponding author(s). E-mail(s): xiangsh@mail.csu.edu.cn;
Contributing authors: clonezhao.1994@gmail.com;

Abstract

A novel barycentric interpolation algorithm with a specific exponential convergence rate is designed for analytic functions defined on the complex plane, with singularities located near the interpolation region, where the region is compact and can be disconnected or multiconnected. The core of the method is the efficient computation of the interpolation nodes and poles using discrete distributions that approximate the equilibrium logarithmic potential, achieved by solving a Symm's integral equation. It takes different strategies to distribute the poles for isolated singularities and branch points, respectively. In particular, if poles are not considered, it derives a polynomial interpolation with exponential convergence. Numerical experiments illustrate the superior performance of the proposed method.

MSC Classification: 30C10 , 30E10 , 41A20 , 65E05

1 Introduction

Interpolation is one of the most fundamental and commonly used tools in scientific computing, and polynomial interpolation serves as a basic method of approximation across a wide range of numerical analysis [1, 2]. The barycentric

2 *Barycentric Interpolation Based on Equilibrium Potential*

polynomial interpolation formula of the second kind with degree n ,

$$p(x) = \sum_{k=0}^n \frac{w_k}{x - x_k} f(x_k) \bigg/ \sum_{k=0}^n \frac{w_k}{x - x_k}, \quad w_k = C / \prod_{j=0, j \neq k}^n (x_k - x_j), \quad C \neq 0 \quad (1)$$

provides a fast and stable algorithm in approximation [3, 4]. Here, f represents the function being approximated, $\{w_k\}_{k=0}^n$ and distinct points $\{x_k\}_{k=0}^n$ are two sets associated with the weights and nodes, respectively.

The barycentric interpolant (1) is uniquely determined by $\{(x_k, f(x_k))\}_{k=0}^n$ and can be done in a few lines of code by Chebfun [5] to get exponential convergence if f is analytic in a neighborhood of the interpolation region E when E is an interval and $\{x_k\}_{k=0}^n \subset E$ are chosen to be the roots of orthogonal polynomials [2, 6–12]. However, when the interpolation region E is not a line segment, or the singularities of f are close to E , the choice of the interpolation nodes may become difficult, and in these cases, barycentric rational interpolation may provide much faster convergence rates when compared to the polynomial analogues.

From the barycentric polynomial formula (1), it is easy to obtain a rational interpolation form

$$r(x) = \sum_{k=0}^n \frac{w_k f_k}{x - x_k} \bigg/ \sum_{k=0}^n \frac{w_k}{x - x_k}, \quad f_k = f(x_k), \quad w_k \neq 0, \quad (2)$$

which was first proposed by Schneider and Werner in 1986 [13]¹. From (2), we see that the weights $\{w_k\}$ can be independent of $\{x_k\}$. Thus, the rational case has n additional degrees of freedom and is more flexible and robust compared with the polynomial case (1).

The initial exploration of barycentric rational interpolation started with special weights to avoid poles as well as unreachable points in the interpolated region, see Berrut [14]. Another efficient approach is the Floater-Hormann scheme [15, 16] by blending local approximations to form a global one to obtain high orders for smooth functions. These methods only rely on the choice of $\{x_k\}$ in the interval E , where $\{w_k\}$ are selected in special ways [17].

For analytic function $f(x) \in \mathcal{A}([-1, 1])$ with singularities near the interpolation interval, more targeted methods are available if these singularities are known. Tee and Trefethen [18] constructed a conformal mapping to handle the case where there are a pair of conjugate singularities. For functions with more singularities, Hale and Tee [19] utilized the special geometry of the slit regions to enable the use of the Schwarz-Christoffel mapping. These methods expand the Bernstein ellipse of $f \circ g$ by constructing a conformal mapping g , then the rational interpolation at nodes $\{g(x_k)\}$ satisfies $O(|r[f] - f|) = O(|p[f \circ g] - f \circ g|)$ [20], which ensures faster exponential convergence. The poles play an important role in these methods.

¹If $w_k = C / \prod_{j=0, j \neq k}^n (x_k - x_j)$, the interpolant $r(x)$ (2) degenerates to a polynomial interpolant.

To make better use of the extra n degrees of freedom, an extremely powerful AAA (adaptive-Antoulas-Anderson) method has been recently developed [21] for interpolation region E in the complex plane. Given a finite sample set $Z \subseteq \mathbb{C}$ and $f(z)$ for all $z \in Z$, the AAA method selects some of these points as interpolation nodes in a greedy manner, while the remaining points are used as support points to determine the weights $\{w_k\}$. Since this method is without any restriction on the sample set Z , it can be applied to various cases on the complex plane. However, the AAA method does not provide guidance on how to choose the sample points. Therefore, to obtain a better approximation of the function f as a whole, a large number of sample points may be required.

It is worthy of noting that the rational function $r_{n,m}$ ($m \leq n$) can always be rewritten as $r_{n,m}(x) = p_n(x)/q_m(x)$ with $q_m(x) = \prod_{i=1}^m (x - z_i)$ if the poles $\{z_i\}_{i=1}^m$ are given. In addition, the numerator and the denominator can be expressed as n -degree barycentric polynomial forms

$$p_n(x) = \frac{\sum_{k=0}^n \frac{\lambda_k}{x - x_k} p_n(x_k)}{\sum_{k=0}^n \frac{\lambda_k}{x - x_k}}, \quad q_m(x) = \frac{\sum_{k=0}^n \frac{\lambda_k}{x - x_k} q_m(x_k)}{\sum_{k=0}^n \frac{\lambda_k}{x - x_k}}, \quad \lambda_k = \prod_{j=0, j \neq k}^n \frac{1}{x_k - x_j},$$

then $r_{n,m}$ can be represented as

$$r_{n,m}(x) = \sum_{k=0}^n \frac{\lambda_k p_n(x_k)}{x - x_k} \bigg/ \sum_{k=0}^n \frac{\lambda_k q_m(x_k)}{x - x_k} = \sum_{k=0}^n \frac{w_k}{x - x_k} r_{n,m}(x_k) \bigg/ \sum_{k=0}^n \frac{w_k}{x - x_k},$$

where

$$w_k = C \frac{\prod_{i=1}^m (x_k - z_i)}{\prod_{j=0, j \neq k}^n (x_k - x_j)}$$

and C is a non-zero constant [22]. If the interpolation nodes $\{x_j\}$ and poles $\{z_i\}$ are determined and $r_{n,m}(x_k) = f_k$, then the rational interpolation can be represented as

$$r_{n,m}(x) = \sum_{k=0}^n \frac{w_k f_k}{x - x_k} \bigg/ \sum_{k=0}^n \frac{w_k}{x - x_k}, \quad w_k = C \frac{\prod_{i=1}^m (x_k - z_i)}{\prod_{j=0, j \neq k}^n (x_k - x_j)}, \quad C \neq 0. \quad (3)$$

The rational interpolant (3) degenerates to a polynomial if the poles $\{z_i\}$ are not considered.

The effectiveness of (3) is contingent on the provision of $n + 1$ interpolation nodes and m poles, distributed in a thoughtful manner. An arbitrary placement of these nodes and poles could result in a build-up of rounding errors and sluggish convergence.

In this paper, we introduce a novel method for efficiently and directly determining the nodes and poles of the rational interpolation (3). The new approach is established by utilizing a particular discrete density approximation based on the equilibrium logarithmic potential, which involves solving a Symm's integral

4 Barycentric Interpolation Based on Equilibrium Potential

equation. The new method guarantees exponential convergence when approximating analytic functions $f \in \mathcal{A}(E)$, where E is a compact set in the complex plane with a piecewise-smooth boundary ∂E .

Figure 1 depicts the proposed method's application to approximate $f \in \mathcal{A}(E)$ without accounting for poles (i.e., (3) is an interpolation polynomial) in the ‘lollipop’ and ‘ice cream cone’ regions, respectively. The first row of Figure 1 displays the distribution of the 201 polynomial interpolation nodes, while the second row shows the absolute errors of the polynomial interpolation for analytic functions $f(z) = e^{z^2}$, $\frac{1}{2+z^2}$, and $\frac{1}{3+2z^2}$ in the ‘lollipop’, and $f(z) = e^{z^2}$, $\frac{1}{1-z^2}$, and $\frac{1}{z^2}$ in the ‘ice cream cone’, respectively.

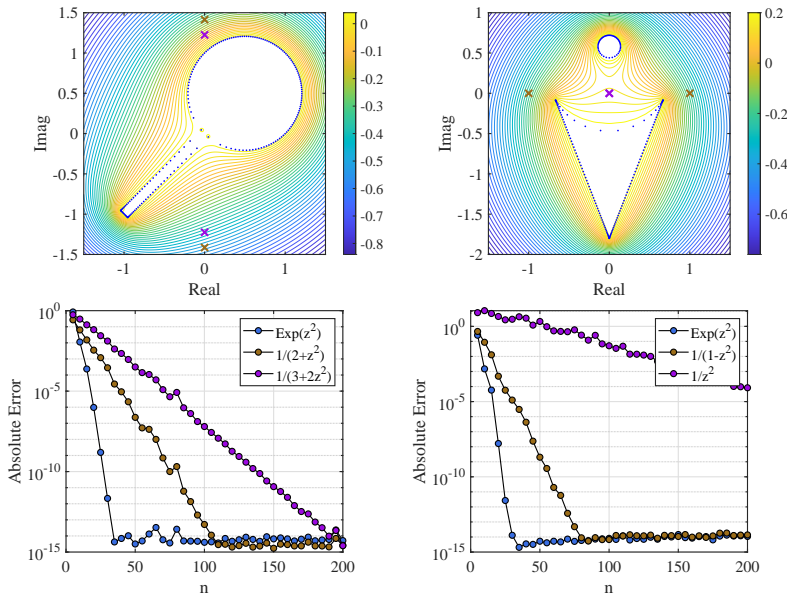


Fig. 1 Potential contours of the nodes ($n = 200$) and absolute errors of polynomial interpolation are shown for $n = 5 : 5 : 200$ in the ‘lollipop’ (left column) and ‘ice cream cone’ (right column) domains.

For $f \in \mathcal{A}(E)$ with singularities near E , rational interpolation with prescribed poles is much better than polynomial interpolation, especially when the location and type of singularities near E are known. To construct the rational interpolant (3) with exponential convergence, we set a compact region F that is disjoint with E , then obtain a discrete distribution that approximate the equilibrium logarithmic potential and find the interpolated nodes on ∂E and poles on the piecewise-smooth boundary ∂F . See Figure 2 for illustrations.

Figure 3 illustrates the rational interpolation approximation of $f(z) = [(z^2 - 0.25)/(z^2 - 0.01)]^{0.5}$ using the proposed method in a disconnected region E . We compare the results with the AAA method using 10^4 random sample points and the polynomial interpolation (3) without consideration of F . The

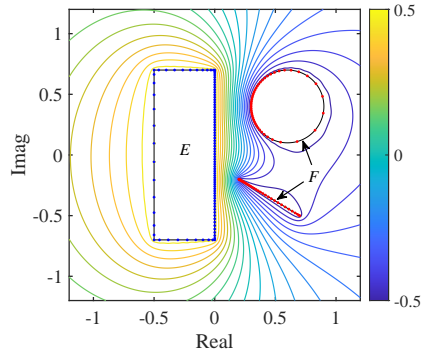


Fig. 2 By our method, the nodes (blue) and poles (red) are selected on ∂E and ∂F , respectively. These nodes $\{x_i\}_{i=0}^n$ and poles $\{z_j\}_{j=1}^m$ make the discrete potential $U(z) = \frac{1}{n+1}(\sum_{i=0}^n \log \frac{1}{|z-x_i|} - \sum_{j=1}^m \log \frac{1}{|z-z_j|})$ almost constant on E and F . Therefore, the interior of E and F is almost blank in the contour map of the potential U .

region E is comprised of a circle and a trapezoid, with the center and radius of the circle being $-0.25 + 0.16i$ and 0.15 , respectively. The four vertices of the trapezoid are $[0.4 - 0.4i, -0.02i, -0.4 - 0.02i, -0.4 - 0.4i]$, and f has four branch points and two branch cuts, one of which is between the circle and the trapezoid. For the rational interpolation (3), we select $F = [-0.5, -0.1] \cup [0.1, 0.5]$.

The convergence of the three methods are presented on the left side of Figure 3, while the nodes, poles, and corresponding potential contours for the rational interpolation based on equilibrium potential are shown on the right side, with $n = 200$. With the proposed method, f can be approximated to machine precision.

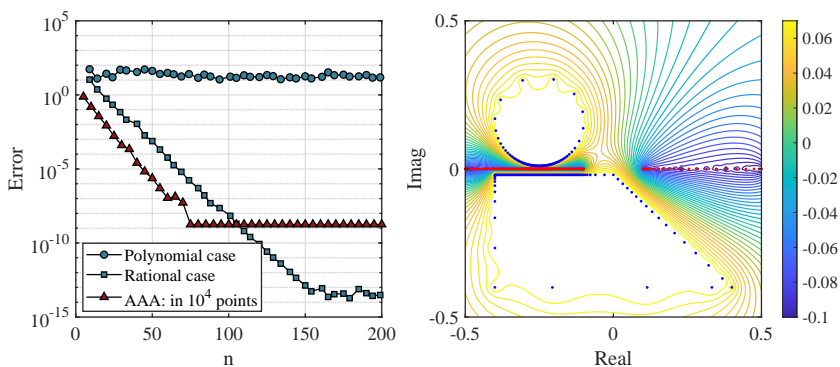


Fig. 3 Left: Absolute errors for $n = 5 : 5 : 200$. Right: The local potential contour with nodes (blue) and poles (red) of $n = 200$.

6 *Barycentric Interpolation Based on Equilibrium Potential*

In addition, the family of interpolation point sets $\{x_i^{(n)}\}_{i=0}^n \subseteq \partial E$ ($n = 1, 2, \dots$) obeys a density function w ($w > 0$) of a unit measure μ on ∂E and satisfies

$$\lim_{n \rightarrow \infty} \max_{1 \leq i \leq n} |x_{i-1}^{(n)} - x_i^{(n)}| = 0.$$

Moreover, the corresponding discrete density measure μ_{n+1} fulfils

$$\lim_{n \rightarrow \infty} \int g \, d\mu_{n+1} = \int g \, d\mu$$

for arbitrary continuous function g on ∂E , where $\mu_{n+1} = 1/(n+1) \sum_{i=0}^n \delta_{x_i}$ and δ_z denotes the Dirac measure at z .

The rest of this paper is organized as follows. In Section 2, we analyze the exponential convergence of the rational interpolation method consistent with the equilibrium potential. Section 3 details the implementation and algorithms of the rational interpolation, while Section 4 demonstrates the effectiveness of the method through various numerical examples. We further discuss on the choice of F in Section 5, and present some concluding remarks in Section 6.

The numerical examples throughout this paper are implemented using Matlab on a laptop with an Intel(R) Core(TM) processor and 8 GB of RAM, and the absolute error refers to the uniform norm error $\|f - r_{n,m}\|_\infty$ over a sufficiently large number of representative sample points on E . Specifically, these points used to estimate the error are mainly distributed on the boundary of E and more points will be placed on the boundary near the singularities. Except for the simplest case $E = [-1, 1]$, we test the error on $-1 : 0.00001 : 1$.

2 Potential theory and convergence

2.1 Potential theory in polynomial approximation

To avoid the Runge phenomenon, polynomial interpolation is made consistent with equilibrium potential [2, 3]. For Lagrange interpolation, the error is expressed as an integral via the Hermite integral formula.

Theorem 1 (Hermite integral formula [2, 23]) *Let P_n be a polynomial interpolation of function f on distinct points $x_0, x_1, \dots, x_n \in E$, and E is a compact set. If f is analytic in the region Ω including E , then for any closed curve Γ in Ω strictly containing E , and x is enclosed by Γ , the following identity is satisfied*

$$f(x) - P_n(x) = \frac{1}{2\pi i} \int_{\Gamma} \frac{l_{n+1}(x)}{l_{n+1}(t)} \frac{f(t)}{(t-x)} dt, \quad (4)$$

where $l_{n+1}(x) = \prod_{i=0}^n (x - x_i)$.

At the right-hand side of (4), $l_{n+1}(x)/l_{n+1}(t)$ is related to the choice of interpolation points and independent of f . If the analytic function f is given and define

$$\|g\|_{\Delta} = \sup_{t \in \Delta} |g(t)|, \quad \Delta \subseteq \mathbb{C},$$

then the asymptotic error of its polynomial interpolation can be completely controlled by the value of the ratio

$$|f(x) - P_n(x)| \leq M \|l_{n+1}\|_E \left\| \frac{1}{l_{n+1}} \right\|_\Gamma, \quad x \in E, \quad (5)$$

where $M = 1/(2\pi) \sup_{x \in E} \int |f(t)/(t-x)| d\nu_\Gamma(t)$, ν_Γ is a measure that satisfies $\nu_\Gamma(S) = |S \cap \Gamma|_L$ for all $S \subseteq \mathbb{C}$, and $|S \cap \Gamma|_L$ denotes the length of $S \cap \Gamma$. For simplicity of expression, we use $\int_\Gamma |dt|$ to denote $\int d\nu_\Gamma(t)$ if it does not create confusion.

From (5), the interpolation error can be estimated by a logarithmic potential [2, 24, 25].

Definition 1 (Logarithmic Potential [24]) Let $\mathcal{M}(E)$ be the set of all unit measures on the region E . For any measure $\mu \in \mathcal{M}(E)$, $U^\mu(z) = \int_E -\log|z-t| d\mu(t)$ is the logarithmic potential function with respect to μ .

Let μ_{n+1} be defined by $\mu_{n+1} = 1/(n+1) \sum_{i=0}^n \delta_{x_i}$. Then it follows

$$|l_{n+1}(x)| = [\exp(-U^{\mu_{n+1}}(x))]^{n+1}, \quad x \in E; \quad |l_{n+1}(t)| = [\exp(-U^{\mu_{n+1}}(t))]^{n+1}, \quad t \in \Gamma,$$

and from (5), we have

$$|f(x) - P_n(x)| \leq M [\exp(\|U^{\mu_{n+1}}\|_\Gamma - \inf_{x \in E} |U^{\mu_{n+1}}(x)|)]^{n+1}. \quad (6)$$

Thus, suppose that $\mu_E \in \mathcal{M}(E)$ is an equilibrium measure and $U^{\mu_E}(x) = C$ for $x \in E$, and that $\mu_{n+1} \Rightarrow \mu_E$, i.e., $\lim_{n \rightarrow \infty} \int_E g d\mu_{n+1} = \int_E g d\mu$ for all continuous function g on E , then it indicates

$$\limsup_{n \rightarrow \infty} |f(x) - P_n(x)|^{\frac{1}{n+1}} \leq \exp(\|U^{\mu_{n+1}}\|_\Gamma - C), \quad x \in E,$$

and deduces

$$\limsup_{n \rightarrow \infty} |f(x) - P_n(x)|^{\frac{1}{n+1}} \leq \rho, \quad x \in E, \quad (7)$$

where $\rho = \exp(\inf_\Gamma \|U^{\mu_E}\|_\Gamma - C)$. Interestingly, the equilibrium potential $U^{\mu_E}(z)$ takes the maximum value C on E [24, 25]. In particular, from the definition of $U^{\mu_E}(z)$, the farther z is from E , the smaller is the value of its potential function $U^{\mu_E}(z)$. Then $\rho < 1$ and the polynomial interpolation satisfying $\mu_{n+1} \Rightarrow \mu_E$ converges at an exponential rate.

2.2 Exponential convergence of rational interpolation of type (n, m)

Analogous to the polynomial interpolation, we present an exponential convergence of rational interpolation that is consistent with equilibrium potential

via Hermite integral. Hermite integral formula for rational interpolation was introduced in Walsh [23, §8.1, Chapter 8].

Theorem 2 (*Hermite integral formula for rational [23, Theorem 2, P. 186]*) Let \mathcal{C} be a closed limited region or several closed limited regions whose boundary Γ consists of a finite number of non-intersecting rectifiable Jordan curves, let the points x_0, \dots, x_n lie interior to \mathcal{C} , and let f be analytic in \mathcal{C} . If $r(z)$ denotes the rational function of degree n whose poles lie in the points z_1, \dots, z_n , and which interpolates to $f(z)$ in $\{x_i\}_{i=0}^n$, distinct from $\{z_i\}_{i=1}^n$. Then we have for any $x \in \mathcal{C}$ and $x \neq z_i$,

$$f(x) - r(x) = \frac{1}{2\pi i} \int_{\Gamma} \frac{\prod_{i=0}^n (x - x_i) \prod_{j=1}^n (t - z_j)}{\prod_{i=0}^n (t - x_i) \prod_{j=1}^n (x - z_j)} \frac{f(t)}{t - x} dt. \quad (8)$$

In (8), points z_i may lie in \mathcal{C} and of course points z_i may be infinite; in the latter case, the factors containing z_i in (8) are simply to be omitted [23, P. 186]. Then it directly leads to the following result.

Corollary 3 Let E be a compact set in \mathbb{C} whose boundary ∂E consists of a finite number of non-intersecting rectifiable Jordan curves and is piecewise-smooth, strictly bounded by a closed curve Γ , and let f be analytic in E and can be extended continuously to Γ . Suppose $r_{n,m}$ (3) is the rational function with simple poles at $\{z_j\}_{j=1}^m$ ($m \leq n$) that interpolates f at distinct points $\{x_i\}_{i=0}^n$. Then for any $x \in E$,

$$f(x) - r_{n,m}(x) = \frac{1}{2\pi i} \int_{\Gamma} \frac{\phi_{n+1,m}(x)}{\phi_{n+1,m}(t)} \frac{f(t)}{t - x} dt, \quad (9)$$

where

$$\phi_{n+1,m}(x) = \prod_{i=0}^n (x - x_i) / \prod_{j=1}^m (x - z_j).$$

Similar to (5), we have

$$|f(x) - r_{n,m}(x)| \leq M \|\phi_{n+1,m}\|_E \left\| \frac{1}{\phi_{n+1,m}} \right\|_{\Gamma}, \quad x \in E. \quad (10)$$

To get exponential convergence of the rational interpolation (3), we will choose a compact set F with piecewise smooth boundary ∂F such that E and F are disjoint.

Suppose μ_E and μ_F are two positive measures on E and F , respectively, and satisfy $\mu_E(E) = 1$ and $\mu_F(F) = \gamma$, where $0 < \gamma < 1$. Define a signed measure $\mu[E, F, \gamma]$ on (E, F) as $\mu[E, F, \gamma](S) = \mu_E(S) - \mu_F(S)$ for all $S \subseteq \mathbb{C}$, and the logarithmic potential of the signed measure as

$$U^{\mu[E, F, \gamma]}(z) = \int \log \frac{1}{|z - t|} d\mu_E(t) - \int \log \frac{1}{|z - t|} d\mu_F(t).$$

Let the discrete measure $\mu_{n+1,m} = \mu[\{x_k^{(n)}\}_{k=0}^n, \{z_i^{(n)}\}_{k=1}^m, \frac{m}{n+1}]$ be defined by

$$\mu_{n+1,m} = \frac{1}{n+1} \sum_{k=0}^n \delta_{x_k^{(n)}} - \frac{1}{n+1} \sum_{k=1}^m \delta_{z_k^{(n)}} \quad (11)$$

with $\{x_k^{(n)}\}_{k=0}^n \in \partial E$ and $\{z_k^{(m)}\}_{k=1}^m \in \partial F$, respectively. It is easy to show that $|\phi_{n+1,m}(z)|^{\frac{1}{n+1}} = \exp(-U^{\mu_{n+1,m}}(z))$, and the error (10) can be expressed as

$$|f(x) - r_{n,m}(x)| \leq M \left[\exp(\|U^{\mu_{n+1,m}}\|_{\Gamma} - \inf_{x \in E} |U^{\mu_{n+1,m}}(x)|) \right]^{n+1}, \quad x \in E. \quad (12)$$

Suppose $\text{supp}(\mu_E) = \partial E$, $\text{supp}(\mu_F) = \partial F$, and $\mu[E, F, \gamma]$ satisfies

$$U^{\mu[E,F,\gamma]}(z) = \begin{cases} c_1, & z \in E \\ -c_2, & z \in F \end{cases}, \quad c_1 > -c_2, \quad (13)$$

and

$$\mu_{n+1,m} = \mu \left[\{x_k^{(n)}\}_{k=0}^n, \{z_k^{(m)}\}_{k=1}^m, \frac{m}{n+1} \right] \Rightarrow \mu[E, F, \gamma], \quad \frac{m}{n+1} \rightarrow \gamma, \quad n \rightarrow \infty, \quad (14)$$

then by (12), we have for $x \in E$ that

$$\limsup_{n \rightarrow \infty} |f(x) - r_{n,m}(x)|^{\frac{1}{n+1}} \leq \exp \left(\|U^{\mu[E,F,\gamma]}(t)\|_{\Gamma} - c_1 \right),$$

and consequently

$$\limsup_{n \rightarrow \infty} |f(x) - r_{n,m}(x)|^{\frac{1}{n+1}} \leq \exp \left(\inf_{\Gamma} \|U^{\mu[E,F,\gamma]}(t)\|_{\Gamma} - c_1 \right). \quad (15)$$

- In the case that f can be continued analytically to $\mathbb{C} \setminus F$: From $|\phi_{n+1,m}(z)| \rightarrow +\infty$ as $|z| \rightarrow \infty$, we have $U^{\mu_{n+1,m}}(z) \rightarrow -\infty$ as $|z| \rightarrow \infty$. Consequently, for sufficiently large n , we can always find Γ around E disjoint F satisfying $U^{\mu[E,F,\gamma]}$ equal to $\varepsilon - c_2$ on Γ for arbitrary $\varepsilon > 0$. Then it yields $\inf_{\Gamma} \|U^{\mu[E,F,\gamma]}(t)\|_{\Gamma} = -c_2$ and

$$\limsup_{n \rightarrow \infty} |f(x) - r_{n,m}(x)|^{\frac{1}{n+1}} \leq \exp(-c_2 - c_1). \quad (16)$$

- In the case that f is not analytic over a set χ with $E \subseteq \chi \subseteq \mathbb{C} \setminus F$, the exponential convergence (15) still holds, but where $\inf_{\Gamma} \|U^{\mu[E,F,\gamma]}(t)\|_{\Gamma} = \sup\{U^{\mu[E,F,\gamma]}(z) : z \in (\chi \cup F)\}$.

Here, the rational functions $\{r_{n,m(n)}\}_{n=0}^{\infty}$ is called a ray sequence if $m(n)/n \rightarrow \theta \in (0, 1]$ as $n \rightarrow \infty$. For a rigorous treatment of the ray sequence, the reader is referred to [26].

Note that the desired non-zero measure is confined to the boundaries of E and F due to the fact that the potentials inside E and F are fully determined by the boundary potentials. As a result, the nodes and poles must be selected on the boundaries of E and F , respectively.

To achieve the exponential convergence of the rational interpolation (3) that is consistent with the equilibrium potential, we must solve three key problems:

- (i) How should F be chosen?
- (ii) How to evaluate $\mu[E, F, \gamma]$ or the density function w of the equilibrium potential?
- (iii) How can the point distribution that satisfies (14) be obtained?

It is worthy of noticing that if F is not considered, the rational interpolant degenerates to a polynomial interpolant. In the following section, we will thoroughly address these issues.

3 Algorithms of the rational interpolation

We will discuss how to obtain a family of point sets $\{\{x_k^{(n)}\}_{k=0}^n : n = 1, 2, \dots\} \subseteq \partial E$ such that $\mu_{n+1} = 1/(n+1) \sum_{i=0}^n \delta_{x_i} \Rightarrow \mu$ for a given $\mu \in \mathcal{M}(E)$ satisfying $\text{supp}(\mu) = \partial E$, where μ_{n+1} is also a unit measure corresponding to the point set $\{x_k^{(n)}\}_{k=0}^n$. These discussions can also be applied to region F .

Suppose w is the density function of unit positive measure μ (i.e., $\int_{\partial E} w(t) |dt| = 1$) and $w(t) > 0$ for all $t \in \partial E$.

Definition 2 A family of point sets $\{\{x_k^{(n)}\}_{k=0}^n : n = 1, 2, \dots\}$ obeys the density function $w(t) > 0$ for all $t \in \partial E$ if for any segment $\partial E[\widehat{a}, \widehat{b}] \subseteq \partial E$, the family of point sets satisfies

$$\lim_{n \rightarrow \infty} \frac{n_{\partial E[\widehat{a}, \widehat{b}]}}{n+1} = \int_{\partial E[\widehat{a}, \widehat{b}]} w(t) |dt|, \quad (17)$$

where a and b are the two endpoints of the segment $\partial E[\widehat{a}, \widehat{b}]$ and $n_{\partial E[\widehat{a}, \widehat{b}]}$ denotes the number of the points on $\partial E[\widehat{a}, \widehat{b}]$.

Theorem 4 If ∂E is a bounded piecewise simply smooth boundary and a family of point sets $\{x_i^{(n)}\}_{i=0}^n \subseteq \partial E$ obeys a positive density function w of a unit measure μ on ∂E , then it holds

$$\lim_{n \rightarrow \infty} \max_{1 \leq i \leq n} |x_{i-1}^{(n)} - x_i^{(n)}| = 0 \quad (18)$$

and $\mu_{n+1} \Rightarrow \mu$, i.e.,

$$\lim_{n \rightarrow \infty} \int g d\mu_{n+1} = \int g d\mu \quad (19)$$

for arbitrary continuous function g on ∂E , where $\mu_{n+1} = 1/(n+1) \sum_{i=0}^n \delta_{x_i^{(n)}}$.

For consistency of the implementation of the rational interpolation, we sketch Theorem 4 in Appendix A.

In this paper, the family of the point sets is chosen such that for any two adjacent points $x_i^{(n)}, x_{i+1}^{(n)} \in \{x_k^{(n)}\}_{k=0}^n$, it holds

$$\int_{\partial E[\widehat{x_i^{(n)}, x_{i+1}^{(n)}}]} w(t) |dt| = \begin{cases} 1/(n+1), & \partial E \text{ is a closed curve, } i = 0, 1, \dots, n \\ 1/n, & \partial E \text{ is a curve segment, } i = 0, \dots, n-1 \end{cases},$$

where $x_{n+1}^{(n)} = x_0^{(n)}$ for ∂E is a closed curve. It is easy to verify that $\{x_i^{(n)}\}_{i=0}^n$ satisfies (17). Then the above equation can be expressed as

$$\int_{\partial E[\widehat{x_0^{(n)}, x_i^{(n)}}]} w(t) |dt| = \begin{cases} i/(n+1), & \partial E \text{ is a closed curve} \\ i/n, & \partial E \text{ is a curve segment} \end{cases}, \quad i = 0, 1, \dots, n. \quad (20)$$

If ∂E is a closed curve, $x_0^{(n)}$ could be any point on ∂E . If ∂E is a curve segment, $x_0^{(n)}$ is an endpoint of the curve segment.

As an example, we consider the density function $w(t) = (\pi\sqrt{1-x^2})^{-1}$ on $E = [-1, 1]$. Suppose a family of point sets $\{\{x_k^{(n)}\}_{k=0}^n : n = 1, 2, \dots\}$ on E satisfies (20). It yields

$$x_i^{(n)} = \cos\left(\frac{n-i}{n}\pi\right), \quad (21)$$

and we obtain the Chebyshev-Lobatto points.

However, getting an explicit formula for the density function w of the equilibrium measure can be challenging, especially for general regions E and F with various shapes and relative positions. Moreover, even if an analytical expression for the density function is obtained, it may not be possible to explicitly express the point distribution from (20). To overcome these challenges, we will apply a step function $\hat{w}(t)$ to approximate the density function $w(t)$ by solving a Symm's integral equation.

3.1 Polynomial interpolation based on equilibrium potential

The most straightforward scenario is polynomial interpolation with poles situated at infinity in the complex plane. In this case, we can obtain an estimation of the equilibrium potential's density function, \hat{w} , by solving Symm's integral equation [27]

$$\int_{\partial E} \log \frac{1}{|z-t|} w(t) |dt| = c_1, \quad z \in E, \quad (22)$$

where w is the density function of the equilibrium measure and satisfies

$$\int_{\partial E} w(t) |dt| = 1. \quad (23)$$

Here E could be a finite union of simply connected compact regions with piecewise-smooth boundaries.

Numerous numerical methods have been developed to solve Symm's integral equations [27, Chapter 9]. In this work, we utilize the constant element method to solve (22) and (23). This method is straightforward to implement and provides an approximation in the form of a step function.

We partition ∂E into N segments, $\partial E_1, \dots, \partial E_N$, using t_1, \dots, t_{N+1} as the dividing points. If the curve is closed, the first and last points coincide. It is noteworthy that N does not depend on n , but increasing N enhances the precision of the density function approximation, yielding more precise discrete points. In our examples, we choose $N = 500$ for simply connected E and F while $N = 3000$ for other cases.

Let $\hat{w}_i (\approx w(t))$ for $t \in \partial E_i$. Taking a point $t_{i+1/2} \in \partial E_i$ in each subinterval ∂E_j , Eq. (22) is simplified to

$$\sum_{j=1}^N \hat{w}_j \int_{\partial E_j} \log \frac{1}{|t_{i+1/2} - t|} |dt| = c_1, \quad i = 1, \dots, N. \quad (24)$$

Then (24) can be represented as $\mathbf{A}\hat{\mathbf{w}} = \mathbf{c}_1$ where $\hat{\mathbf{w}} = [\hat{w}_1; \dots; \hat{w}_N]$, $\mathbf{c}_1 = [c_1; \dots; c_1]$, and the $a_{i,j}$ of \mathbf{A} denotes

$$a_{i,j} \approx \int_{\partial E_j} \log \frac{1}{|t_{i+1/2} - t|} |dt|, \quad i = 1, \dots, N, \quad j = 1, \dots, N.$$

For $i \neq j$, $a_{i,j}$ is evaluated by

$$a_{i,j} = -\frac{|\partial E_i|_L}{6} (\log|t_{i+\frac{1}{2}} - t_j| + 4\log|t_{i+\frac{1}{2}} - t_{j+\frac{1}{2}}| + \log|t_{i+\frac{1}{2}} - z_{j+1}|), \quad (25)$$

while for $i = j$,

$$a_{i,i} = |t_{i+\frac{1}{2}} - t_i| (\log|t_{i+\frac{1}{2}} - t_i| - 1) + |t_{i+\frac{1}{2}} - t_{i+1}| (\log|t_{i+\frac{1}{2}} - t_{i+1}| - 1) \quad (26)$$

(see [27, P. 241]), where $|\partial E_i|_L$ denotes the length of ∂E_i . Then equations (22) and (23) are jointly expressed as

$$\left(\begin{array}{ccc|c} a_{1,1} & \cdots & a_{1,N} & -1 \\ \vdots & \ddots & \vdots & \vdots \\ a_{N,1} & \cdots & a_{N,N} & -1 \\ \hline |\partial E_1|_L & \cdots & |\partial E_N|_L & 0 \end{array} \right) \begin{pmatrix} \hat{w}_1 \\ \vdots \\ \hat{w}_N \\ c_1 \end{pmatrix} = \begin{pmatrix} 0 \\ \vdots \\ 0 \\ 1 \end{pmatrix}. \quad (27)$$

The approximate density $\hat{\mathbf{w}}$ and the potential c_1 can be obtained from (27).

Thereafter, we can obtain the nodes from (20) using the approximate density function $\hat{w}(t) = \hat{w}_i$ for $t \in \partial E_i$. Without loss of generality, we consider a distribution of n points $\{x_i^{(n)}\}_{i=1}^n$ on ∂E . Suppose $\{x_i^{(n)}\}_{i=1}^n$ and the approximate density function $\hat{w}(t)$ satisfies (20) (Note that it is n points here for notational simplicity).

We replace $x_0^{(n)}$ in (20) with $x_1^{(n)}$ and set $x_1^{(n)} = t_1$, and define

$$h_{n,i} = \begin{cases} (i-1)/n, & \partial E \text{ is a closed curve} \\ (i-1)/(n-1), & \partial E \text{ is a curve segment} \end{cases},$$

and $s_j = \sum_{i=1}^j |\partial E_i|_L \hat{w}_i$ for $j = 0, 1, \dots, (N-1)$ ($s_0 = 0$). If $s_{k-1} \leq h_{n,i} < s_k$, then $x_i^{(n)} \in \partial E[\widehat{t_{k-1}, t_k}]$, and (20) can be approximated by

$$\sum_{j=1}^{k-1} |\partial E_j|_L \hat{w}_j + |\partial E[\widehat{t_k, x_i^{(n)}}]|_L \hat{w}_k = h_{n,i}, \quad i = 1, \dots, n. \quad (28)$$

This allows us to express the length of $x_i^{(n)}$ from the starting point $x_1^{(n)} = t_1$ on ∂E as

$$|\partial E[\widehat{t_1, x_i^{(n)}}]|_L = \sum_{j=1}^{k-1} |\partial E_j|_L + \varepsilon_{i,k}, \quad \varepsilon_{i,k} = (h_{n,i} - s_{k-1})/\hat{w}_k.$$

Define matrix $\mathbf{B} = [b_{i,j}]$ ($1 \leq i \leq n, 1 \leq j \leq N$) with

$$b_{i,j} = \begin{cases} 1, & \hat{b}_{i,j} \geq 1 \\ \hat{b}_{i,j}, & 0 < \hat{b}_{i,j} < 1, \quad \hat{b}_{i,j} = \frac{h_{n,i} - s_{j-1}}{|\partial E_j|_L \hat{w}_j} \\ 0, & \hat{b}_{i,j} \leq 0 \end{cases}. \quad (29)$$

It holds

$$[|\partial E[\widehat{t_1, x_1^{(n)}}]|_L, \dots, |\partial E[\widehat{t_1, x_n^{(n)}}]|_L]^T = \mathbf{B}[|\partial E_1|_L, \dots, |\partial E_N|_L]^T. \quad (30)$$

Given a reference point t_1 , the nodes $\{x_i^{(n)}\}_{i=1}^n$ can be obtained from the curve lengths $|\partial E[\widehat{t_1, x_i^{(n)}}]|_L$, where $\partial E[\widehat{t_1, x_i^{(n)}}]$ denotes the part of the boundary of E that connects \hat{t}_1 and $x_i^{(n)}$. Using these nodes, we can perform the barycentric polynomial interpolation using (1).

Algorithm 1 summarizes the above process, while Algorithm 2 outlines the procedure for obtaining the corresponding discrete points from the density function. It is worth noting that when E is a union of simply connected regions,

we tend to divide the boundary of E into multiple parts and use `den2pts` separately for each part, where the ratio of the number of the points in each part approximates the ratio of the integrals of the density function \hat{w} over these parts.

Algorithm 1 Barycentric polynomial interpolation with equilibrium potential

- 1: **function** BPIEP($f \in \mathcal{A}(E)$, $n \in \mathbb{N}$)
 - 2: Discrete ∂E ;
 - 3: Get approximately density function \hat{w} by (27);
 - 4: The nodes $X = \{x_i^{(n)}\}_{i=0}^n \leftarrow \text{den2pts}(\hat{w}, n + 1)$;
 - 5: Return $P_n[f]$ from the polynomial case of (1) with the nodes X .
 - 6: **end function**
-

Algorithm 2 Generate points from density function \hat{w}

- 1: **function** den2pts($\hat{w}, n \in \mathbb{N}$)
 - 2: Normalize \hat{w} and define column vectors $L = [|\partial E[t_i, t_{i+1}]|_L]$, $W = [\hat{w}_i]$;
 - 3: Set $S = [0; |\partial E_1|_L \hat{w}_1; \dots; \sum_{i=1}^{N-1} |\partial E_i|_L \hat{w}_i]$;
 - 4: Compute matrix \mathbf{B} by (29);
 - 5: Return points $\{x_i^{(n)}\}_{i=1}^n$ by (30);
 - 6: **end function**
-

Figure 4 displays several examples of the polynomial interpolation discussed above in an L-shaped region. The six vertices of this L-shaped region are $\exp(-i\pi/4)[0, 1, 1 + 0.5i, 0.5 + 0.5i, 0.5 + 1i, 1i]$. The interpolated functions are $f(z) = \sqrt{z + 0.2}$ with a branch singularity at -0.2 , $f(z) = 1/(z^2 + 0.04)$ with isolated singularities at $\pm 0.2i$, and $f(z) = 1/(z - 1)$ with an isolated singularity at 1. The left of Figure 4 shows the singularities of the interpolated functions and the contours of the discrete potential U generated by the nodes when $n = 300$. The discrete potential U has a value of about 0.1937 at -0.2 (red+), 0.3868 at $\pm 0.2i$ (blue+), and 0.5002 at 1 (black+). The right of Figure 4 shows the convergence rates of the polynomial interpolation of these functions, which are consistent with their theoretical convergence rates.

3.2 Rational interpolation based on equilibrium potential

To approximate an analytic function $f \in \mathcal{A}(E)$ with singularities near E , rational interpolation is much better than the corresponding polynomial interpolation. This is because rational interpolation can introduce poles in the vicinity of the singularities of f , which can accelerate the convergence.

We introduce a region F for distributing the poles of the rational interpolation (3) to approximate analytic functions $f \in \mathcal{A}(E)$ with singularities near E . For specific singularities, we can use simple strategies for selecting F .

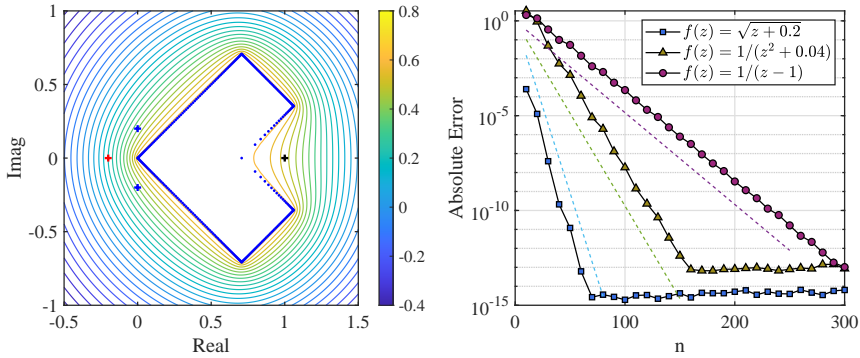


Fig. 4 Left: Interpolation nodes (blue) and the discrete potential U generated by the nodes when $n = 300$. Right: The convergence rates compared with the theoretical convergence rates ρ^n , $\rho = \exp(-0.4180)$ (blue dashed), $\rho = \exp(-0.2248)$ (green dashed) and $\rho = \exp(-0.1115)$ (rosy dashed), respectively.

- When the singular point Z is isolated, such as a pole or essential singularity, we cover it with a small disk $F = D(Z, r)$ to avoid intersection with E and ensure a lower potential on F .
- For branch singularities, if the two endpoints of a branch cut are Z_1 and Z_2 , and Z_1 is close to E but Z_2 is far from E , we make a line segment from Z_1 in the direction away from E . We find that a length between 1 and 4 is often acceptable when the diameter of E is between 1 and 2. For example, set $f(z) = \sqrt{x + 0.1}$ and $E = [0, 1]$. The branch cut is $[Z_2, Z_1] = [-\infty, -0.1]$ and we select $F = [-1.1, -0.1]$.
- For branch singularities, if the two ends of the branch cut $[Z_1, Z_2]$ are both near E , we typically use the line segment $[Z_1, Z_2]$ as F if it does not intersect E . For example, let $f(z) = [(z^2 - 0.25)/(z^2 - 0.01)]^{0.5}$, which has four branch points and two branch cuts. Then we choose $F = [-0.5, -0.1] \cup [0.1, 0.5]$ (see Figure 3). In some cases, it may be useful to use a curved segment as F to avoid intersection with E . See Section 5 for more discussion on the length of F .

Similar to the previous subsection, we still start with the potential. From the properties of the equilibrium potential and (16), we get

$$\int_{\partial E} \log \frac{1}{|z-t|} w_E(t) |dt| - \int_{\partial F} \log \frac{1}{|z-t|} w_F(t) |dt| = \begin{cases} c_1, & z \in \partial E \\ -c_2, & z \in \partial F \end{cases}, \quad (31)$$

and

$$\int_{\partial E} w_E(t) |dt| = 1, \quad \int_{\partial F} w_F(t) |dt| = \gamma, \quad (32)$$

where $w_S(t) > 0$, and S denotes E or F . For the more general case, ∂E and ∂F may consist of multiple simple boundaries.

Let ∂E be divided into I subintervals $\{\partial E_k\}_{k=1}^I$ and ∂F be divided into J subintervals $\{\partial F_k\}_{k=1}^J$. For convenience, $\{\partial E_k\}_{k=1}^I$ and $\{\partial F_k\}_{k=1}^J$ are noted

as $\{\partial S_k\}_{k=1}^N$ ($N = I + J$). Similar to the polynomial case, let $\hat{w}_{E_k}(\approx w_E(t))$ for $t \in \partial E_k$ and $\hat{w}_{F_k}(\approx w_F(t))$ for $t \in \partial F_k$, then (31) and (32) are jointly expressed as

$$\left(\begin{array}{ccc|ccc|cc} a_{1,1} & \cdots & a_{1,I} & -a_{1,I+1} & \cdots & -a_{1,N} & -1 & 0 \\ \vdots & \ddots & \vdots & \vdots & \ddots & \vdots & \vdots & \vdots \\ a_{I,1} & \cdots & a_{I,I} & -a_{I,I+1} & \cdots & -a_{I,N} & -1 & 0 \\ \hline a_{I+1,1} & \cdots & a_{I+1,I} & -a_{I+1,I+1} & \cdots & -a_{I+1,N} & 0 & 1 \\ \vdots & \ddots & \vdots & \vdots & \ddots & \vdots & \vdots & \vdots \\ a_{N,1} & \cdots & a_{N,I} & -a_{N,I+1} & \cdots & -a_{N,N} & 0 & 1 \\ \hline |\partial E_1|_L & \cdots & |\partial E_I|_L & 0 & \cdots & 0 & 0 & 0 \\ 0 & \cdots & 0 & |\partial F_1|_L & \cdots & |\partial F_J|_L & 0 & 0 \end{array} \right) \begin{pmatrix} \hat{w}_{E_1} \\ \vdots \\ \hat{w}_{E_I} \\ \hat{w}_{F_1} \\ \vdots \\ \hat{w}_{F_J} \\ c_1 \\ c_2 \end{pmatrix} = \begin{pmatrix} 0 \\ \vdots \\ 0 \\ 0 \\ \vdots \\ 0 \\ 1 \\ \gamma \end{pmatrix} \quad (33)$$

where $a_{i,j}$ is generated for ordered pairs $(\partial S_i, \partial S_j)$ by the rules of $a_{i,j}$ in Subsection 3.1. Therefore, we can derive the approximate density function \hat{w}_S used to generate the discrete points and the parameters c_1 and c_2 used to estimate the convergence rate (15).

Using the `den2pts` (Algorithm 2), we can obtain the interpolation nodes $\{x_i^{(n)}\}_{i=0}^n$ and poles $\{z_j^{(n)}\}_{j=1}^m$ from the density function \hat{w} . Subsequently, we can obtain the rational interpolation using (3). We summarize the rational interpolation with equilibrium potential in Algorithm 3.

Algorithm 3 Barycentric rational interpolation with equilibrium potential

- 1: **function** BRIEP($f \in \mathcal{A}(E)$, singularities $[q_i]$ of f , $n \in \mathbb{N}$, $\gamma \in (0, 1)$)
 - 2: Select the regions F to cover $[q_i]$;
 - 3: Discrete ∂E and ∂F ;
 - 4: Get approximately density functions \hat{w}_E and \hat{w}_F by (33);
 - 5: The nodes $X = \{x_i^{(n)}\}_{i=0}^n \leftarrow \text{den2pts}(\hat{w}_E, n + 1)$;
 - 6: The poles $Z = \{z_j^{(n)}\}_{j=1}^m \leftarrow \text{den2pts}(\hat{w}_F, m = \lceil \gamma(n + 1) \rceil)$;
 - 7: Barycentric weights $\{w_k\}$ from (3) with X and Z ;
 - 8: Return $r_{n,m}[f]$ from (3) with weights $\{w_k\}$ and nodes X .
 - 9: **end function**
-

4 Experimental results

To demonstrate the rapid convergence of the proposed rational interpolation method, we focus on function $f \in \mathcal{A}(E)$ with singularities near E .

4.1 On the interval $[-1, 1]$

In this subsection, we study the interpolation of analytic functions that have singularities near $E = [-1, 1]$. We compare our method with the conformal

mapping method proposed by Tee and Trefethen [18], as well as the Floater-Hormann method that interpolates at equidistant nodes [15]. For the latter, we use the implementation *Chebfun*($f(X), 'equi'$) within Chebfun [5]. We compare $\|f - r_{n,m}\|_\infty$ of the absolute error of the corresponding interpolants in $-1 : 0.00001 : 1$.

For $f(x) = \exp(1/(1 + 10^4x^2))$ with essential singularities at $\pm 0.01i$, we demonstrate the absolute errors of the rational interpolation (3) by selecting $F = D(-0.01i, 0.0001) \cup D(0.01i, 0.0001)$ and various degrees n , as shown on the left of Figure 5. On the right of Figure 5, we present the local potential map around the singularities, where the nodes and poles attract each other to cluster closely, leading to a uniformly high potential for E and a uniformly low potential for F . As the degree n increases, the convergence rate of our method gradually approaches the theoretical asymptotic rate, which is consistent with the analysis in Section 2. We also note that our method outperforms the conformal mapping method [18] and Floater-Hormann method [15] in terms of absolute errors, as shown in the numerical experiments.

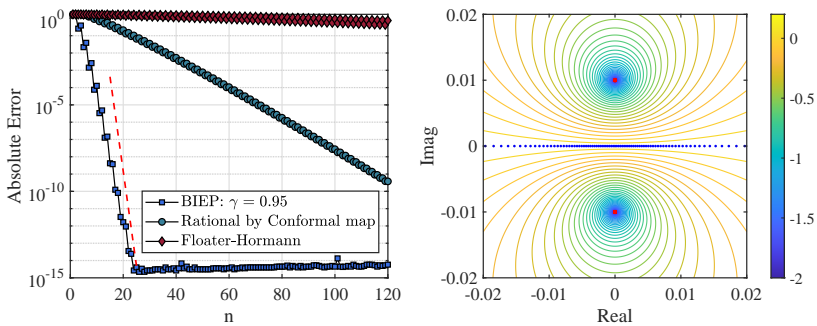


Fig. 5 Left: Absolute errors for $n = 1 : 1 : 120$ together with predicted error slope 0.0807^n (red) obtained by (16). Right: The local potential contour with nodes and poles of our method for $n = 120$.

Figure 6 depicts the convergence behavior of our proposed method with various values of the parameter γ for two different functions: $f(x) = \exp(1/(1+100x^2))$ with essential singularities at $\pm 0.1i$ ($F = D(-0.1i, 0.0001) \cup D(0.1i, 0.0001)$), and $f(x) = \exp(1/(1 + 10^6x^2))$ with singularities at $\pm 0.001i$ ($F = D(-0.001i, 0.0001) \cup D(0.001i, 0.0001)$). The figure illustrates that when γ is small, the error decreases in a stepwise manner since $m = \lfloor \gamma(n + 1) \rfloor$. The results agree with the theoretical asymptotic errors.

Figure 7 illustrates the interpolation approximations of two functions with branch singularities: $f(x) = \exp((1 + 100x^2)^{-0.5})$ with $F = [-0.1i, -2.1i] \cup [0.1i, 2.1i]$ (left) and $f(x) = \exp((1 + 10^4x^2)^{-0.5})$ with $F = [-0.01i, -2.51i] \cup [0.01i, 2.51i]$ (right). The proposed method exhibits faster convergence compared to the two methods.

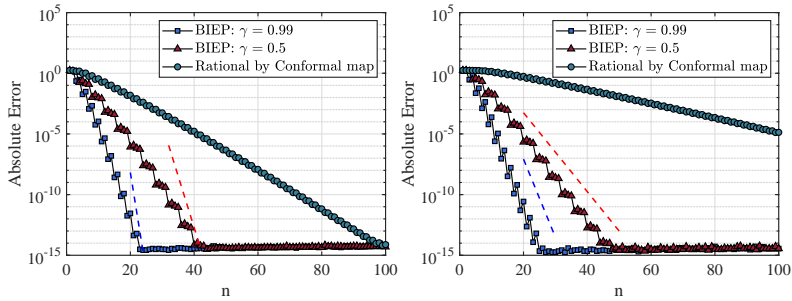


Fig. 6 Left: Absolute errors for $n = 1 : 1 : 100$ together with predicted error slope 0.0231^n (blue) and 0.1419^n (red), respectively. Right: Absolute errors for $n = 1 : 1 : 100$ together with predicted error slope 0.2273^n (blue) and 0.4729^n (red).

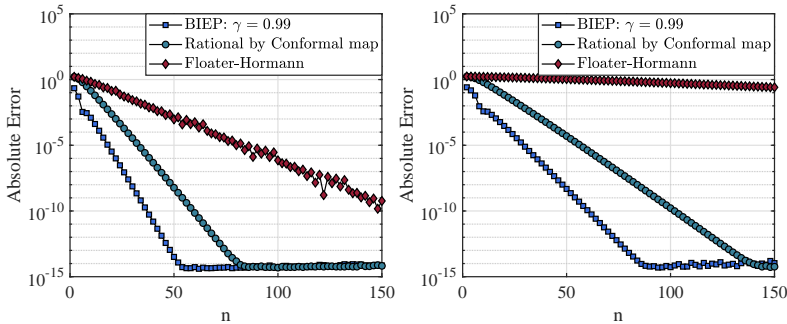


Fig. 7 Left: Absolute errors for $n = 2 : 2 : 150$. Right: Absolute errors for $n = 2 : 2 : 150$.

4.2 On the complex plane region

In this subsection, we present two numerical examples on a square region and an annulus, respectively. We compare the results with the AAA method [21], which is based on randomly sampled points within the region of interest and can produce varying performances. To account for this variability, we conduct five tests and use the median result for comparison.

The first example is on the square region $[-0.5, 0.5] \times [-0.5, 0.5]$ with $f(z) = \exp(1/(5.1^2 + (10z)^2))$, which has two essential singularities at $\pm 0.51i$. In Figure 8, the AAA method converges rapidly and reaches the error tolerance of 10^{-10} with 10^4 random sample points. However, the method does not accurately represent the drastic local changes near the singularities with only 10^4 random sample points. In contrast, the rational interpolation with $F = D(0.510001i, 10^{-6}) \cup D(-0.510001i, 10^{-6})$ converges exponentially as n increases.

The second example concerns an analytic function on a multiconnected region. Such regions are of interest when approximating an analytic function with isolated singularities in the hole. Here, we consider the function $f(z) =$

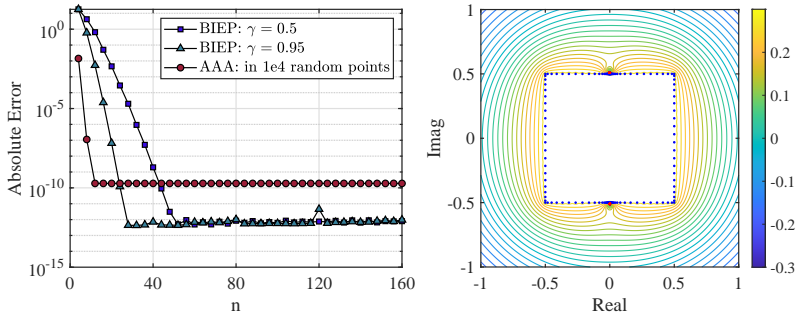


Fig. 8 Left: Absolute errors for $n = 4 : 4 : 160$. Right: The potential contour of the nodes (blue) and poles (red): $n = 160$ and $m = 80$.

$\exp(1/(100(z - 0.09)^{-1}(z - 0.51i)^{-1}))$ defined on the annulus $E = \{re^{2\pi i\theta} : 0.1 \leq r \leq 0.5, 0 \leq \theta < 2\pi\}$. This function has two essential singularities at $0.51i$ and 0.09 , and we cover these singularities with $F = D(0.51i, 10^{-6}) \cup D(0.09, 10^{-6})$. Since some poles of rational interpolation are distributed inside the hole, the interpolation nodes must gather on the inner boundary of E to make the potential on E constant. As shown in Figure 9, both methods perform similarly to the previous examples.

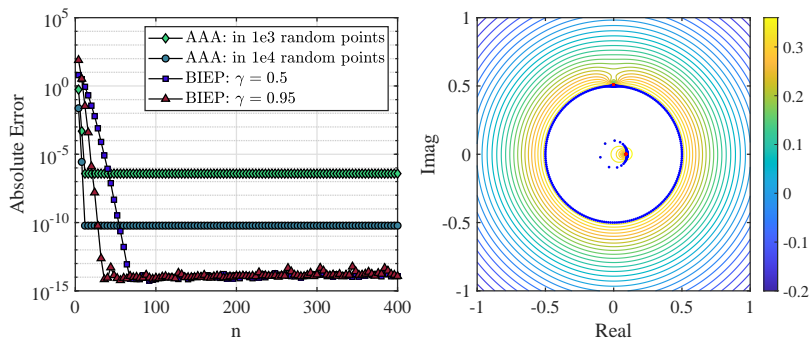


Fig. 9 Left: Absolute errors for $n = 4 : 4 : 400$. Right: The potential contours of the nodes (blue) and poles (red): $n = 400$ and $m = 200$.

While we used the AAA method for comparison, the two have their respective strengths and can complement each other. The former requires prior knowledge about the location and type of singularities of the function f to determine the region F , which can be difficult to obtain in some cases. On the other hand, the AAA method can determine the singularities' location and type and can assist in setting the region F . Then we can use the poles obtained from the AAA method to help determine the region F .

5 Further discussions on the rational interpolation

In Section 3, the parameter that may need to be specified is the length of F for branch singularities. Here, we illustrate this with an example of interpolating the function $f(z) = 1/\sqrt{z}$ on the quadrilateral $[0.1, -0.2+0.5i, 0.7, -0.2-0.5i]$. Figure 10 shows the potential maps when the length of F is 0.5, 2, 4, and 8, from top to bottom.

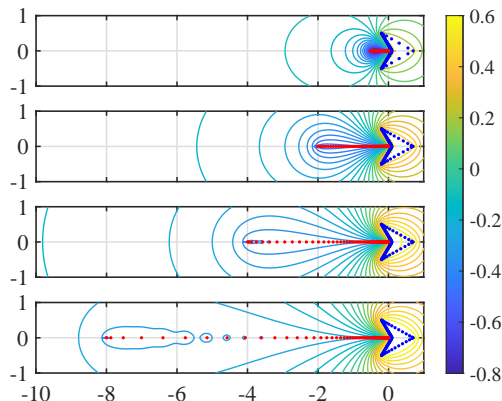


Fig. 10 Potential contours of the nodes (blue) and poles (red) for $n = 100$.

It is worth noting the changes in potential along the path from the left endpoint of F to -10 . The first image clearly shows a significant rise in potential along this path. When compared to other cases with lengths of 2, 4, and 8, respectively, the maximum potential on Γ of (15) will be much larger since Γ cannot cross $[-\infty, 0]$. When the length of F is between 1 and 8, the difference in convergence rate is very slight. This phenomenon is illustrated on the left side of Figure 11. From the right side of Figure 11, this phenomenon is even more evident when we set $\gamma = 0.85$.

Although the convergence rate is not very sensitive to the length of F , a criterion is still needed to determine whether F is appropriate. Figure 12 shows the density functions for the four different lengths of F at $\gamma = 0.99$ and 0.85 , respectively. If the length of F is appropriate, then the end near E will have more poles than the other end. When the approximate density function \hat{w}_F differs by at least one order of magnitude at both ends, the convergence rate is often acceptable.

We consider an example with both isolated singularities and branch points. The boundary curve of the interpolation region E is $z(\theta) = (0.6 + 0.3 \cos(4\theta + \pi)) \exp(i\theta)$, ($0 \leq \theta \leq \pi$). The function $f(z) = \sqrt{z + 0.5}/((z^2 + 0.25)(z - 0.5)) \in \mathcal{A}(E)$ has a branch cut $[-\infty, -0.5]$ and three isolated singularities. We use $[-1, -0.5]$ or $[-2, -0.5]$ for the branch cut. The three isolated singularities

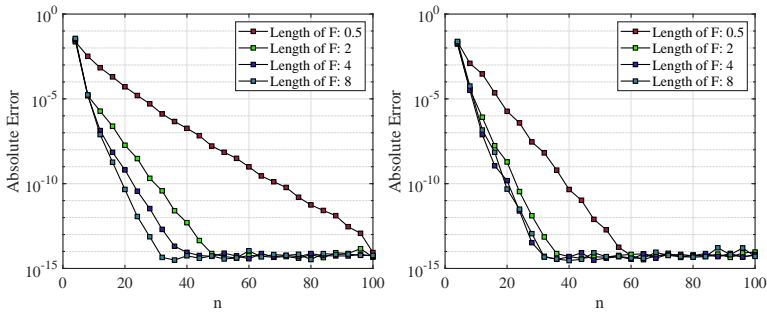


Fig. 11 Absolute errors for $n = 4 : 4 : 100$ with $\gamma = 0.99$ (left) and $\gamma = 0.85$ (right).

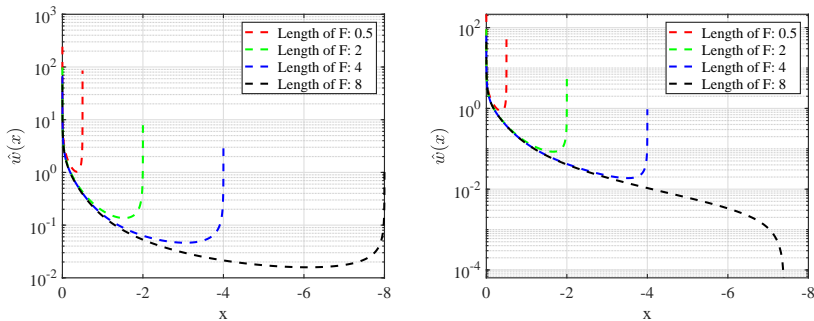


Fig. 12 Left: Density function \hat{w} when $\gamma = 0.99$ (left) and $\gamma = 0.85$ (right). When $\gamma = 0.85$, the density function is negative around -8 if we set the length of F to be 8. Here we just ignore the part where the density function is negative.

are covered by $D(0.5i, 0.01) \cup D(0.5, 0.01) \cup D(-0.5i, 0.01)$ in all cases. The left side of Figure 13 shows the error results and the number of iterations for different F and different γ , respectively.

6 Conclusion

This paper presents an efficient algorithm for the rational interpolation (3) that approximates an analytic function $f \in \mathcal{A}(E)$ or $f \in \mathcal{A}(E)$ with singularities near E with exponential convergence. The interpolation nodes and poles are determined based on the equilibrium logarithmic potential with a specific discrete density approximation obtained by solving a Symm's integral equation.

The method we have presented in this paper has potential applications beyond the realm of rational interpolation with singularities. It can be extended to solve other problems such as the Zolotarev problem on the complex plane or to determine the optimal parameters for the alternating direction implicit (ADI) method [28, 29]. Further research will be conducted in future work.

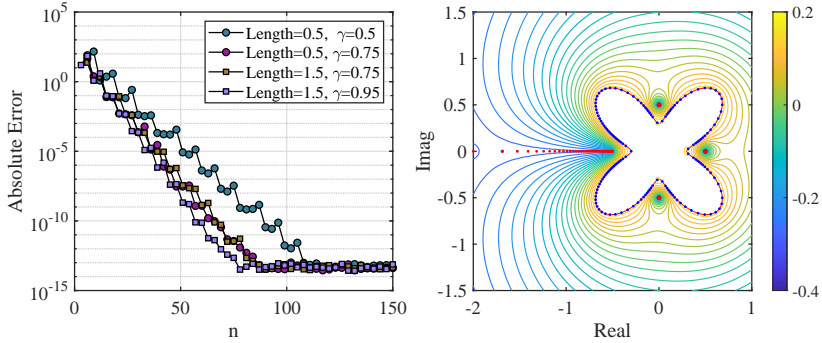


Fig. 13 Left: Absolute error for $n = 3 : 3 : 150$. Right: Potential contour of nodes(blue) and poles(red) of $\gamma = 0.75$.

Appendix A

Proof of Theorem 4: We will first prove (18). Assume that for any positive integer K , there exists $n > K$ such that $\max_{1 \leq i \leq n} |x_{i-1}^{(n)} - x_i^{(n)}| > 2d$ for some positive constant d . Divide ∂E into $m = \lceil |\partial E|_L/d \rceil$ parts $\Gamma_1, \Gamma_2, \dots, \Gamma_m$ with equal length, where $\lceil z \rceil$ denotes the smallest integer greater than or equal to z . Then, for any positive integer K , there exists $n (> K)$ and some $i(n)$ with $1 \leq i(n) \leq m$ such that $n_{\Gamma_{i(n)}} = 0$. Since $\{\Gamma_i\}_{i=1}^m$ are a finite set, thus there is i_0 with $1 \leq i_0 \leq m$ and a subsequence such that $n_{\Gamma_{i(n_k)}} = n_{\Gamma_{i_0}} = 0$ for $k = 1, 2, \dots$, which implies that (17) does not hold, i.e., $\{x_i^{(n)}\}_{i=0}^n$ does not obey $w(t)$ on ∂E since $\lim_{k \rightarrow \infty} \frac{n_{\Gamma_{i(n_k)}}}{n_k} = \int_{\Gamma_{i_0}} w(t) |dt| = \lim_{k \rightarrow \infty} \frac{n_{\Gamma_{i_0}}}{n_k} = 0$, which is contradicted with $\int_{\Gamma_{i_0}} w(t) |dt| > 0$. Then the identity (18) holds.

Next we will show that

$$\lim_{n \rightarrow \infty} \int g d\mu_{n+1} = \int g d\mu \quad (34)$$

for arbitrary continuous function g on ∂E , where $\mu_{n+1} = 1/(n+1) \sum_{i=0}^n \delta_{x_i^{(n)}}$.

Suppose E is a union of simply or multiconnected sets and $\partial E = \bigcup_{i \in I} \partial E^i$, where ∂E^i is close and smooth and I is a finite index set. Then we just need to prove that (34) holds on every ∂E^i .

Denote $\max_{t \in \partial E^i} |g(t)| = G_i$. Let the parametric curve of the smooth curve ∂E^i about the arc length s be $T_i(s)$ ($0 \leq s \leq S_i = |\partial E^i|_L$). Then we have

$$\int_{\partial E^i} g(t) d\mu(t) = \int_{\partial E^i} g(t) w(t) |dt| = \int_0^{S_i} g(T_i(s)) w(T_i(s)) ds.$$

Let $0 = s_0 < s_1 < \dots < s_m = S_i$ satisfy

$$\int_{s_{k-1}}^{s_k} w(T_i(s)) ds = \frac{W_i}{m}, \quad W_i = \int_0^{S_i} w(T_i(s)) ds \leq 1. \quad (35)$$

Since $w > 0$, we have $\lim_{m \rightarrow \infty} \max_{1 \leq k \leq m} |s_k - s_{k-1}| = 0$ from Identity (18).

Note that $g(T_i(s))$ is continuous for $s \in [0, S_i]$. Then for arbitrary $\varepsilon > 0$, there exists K such that

$$\max_{s \in [s_{k-1}, s_k]} g(T_i(s)) - \min_{s \in [s_{k-1}, s_k]} g(T_i(s)) < \frac{\varepsilon}{2}, \quad 1 \leq k \leq m, \quad m \geq K. \quad (36)$$

Given an $m (\geq M)$, by applying the mean value theorem of integration, there exists $\xi_k \in [s_{k-1}, s_k]$ such that

$$\int_0^{S_i} g(T_i(s)) w(T_i(s)) ds = \frac{W_i}{m} \sum_{k=1}^m g(T_i(\xi_k)). \quad (37)$$

Furthermore, from

$$\int_{s_{k-1}}^{s_k} g(T_i(s)) d\mu_{n+1}(T_i(s)) = \frac{\sum_{x \in X_i} g(x)}{n+1}$$

where $X_i = \{x_i^{(n)}\}_{i=0}^n \cap T_i([s_{k-1}, s_k])$, there exists $\zeta_k \in [s_{k-1}, s_k]$ such that

$$\frac{\sum_{x \in X_i} g(x)}{n+1} = g(\zeta_k) \frac{n_{\partial E[\widehat{t}_{k-1}^i, t_k^i]}}{n+1}$$

and

$$|g(T_i(\xi_k)) - g(T_i(\zeta_k))| < \frac{\varepsilon}{2}, \quad (38)$$

where $t_{k-1}^i = T_i(s_{k-1})$ and $t_k^i = T_i(s_k)$.

In addition, from (17), there exists a positive integer N such that for $n > N$

$$\left| \frac{n_{\partial E[\widehat{t}_{k-1}^i, t_k^i]}}{n+1} - \int_{s_{k-1}}^{s_k} w(T_i(s)) ds \right| \leq \frac{\varepsilon m}{2G_i W_i}, \quad k = 1, 2, \dots, m, \quad (39)$$

which, together with (35) and (39), deduces

$$\frac{n_{\partial E[\widehat{t}_{k-1}^i, t_k^i]}}{n+1} \Big/ \int_{s_{k-1}}^{s_k} w(T_i(s)) ds \in \left[1 - \frac{\varepsilon}{2G_i}, 1 + \frac{\varepsilon}{2G_i} \right]. \quad (40)$$

Thus, together with (37), (38) and (40), we have for $n > N$ that

$$\begin{aligned} \left| \int_{\partial E^i} g \, d\mu_{n+1} - \int_{\partial E^i} g \, d\mu \right| &= \left| \sum_{k=1}^m g(T_i(\zeta_k)) \frac{n_{\partial E[t_{k-1}^i, t_k^i]}}{n+1} - \frac{W_i}{m} \sum_{k=1}^m g(T_i(\xi_k)) \right| \\ &\leq \frac{W_i}{m} \sum_{k=1}^m (|g(T_i(\xi_k)) - g(T_i(\zeta_k))| + \frac{\varepsilon}{2G_i} |g(T_i(\zeta_k))|) \\ &\leq \frac{W_i}{m} \sum_{k=1}^m \left(\frac{\varepsilon}{2} + \frac{\varepsilon}{2} \right) \\ &\leq \varepsilon. \end{aligned}$$

This completes the proof.

Funding

This work was supported by the National Natural Science Foundation of China (No. 12271528).

References

- [1] Dahlquist, G., Björck, A.k.: Numerical Methods in Scientific Computing. Vol. I, p. 717. Society for Industrial and Applied Mathematics (SIAM), Philadelphia (2008). <https://doi.org/10.1137/1.9780898717785>. <https://doi.org/10.1137/1.9780898717785>
- [2] Trefethen, L.N.: Approximation Theory and Approximation Practice, p. 305. Society for Industrial and Applied Mathematics (SIAM), Philadelphia (2013)
- [3] Berrut, J.-P., Trefethen, L.N.: Barycentric Lagrange interpolation. SIAM Rev. **46**(3), 501–517 (2004). <https://doi.org/10.1137/S0036144502417715>
- [4] Higham, N.J.: The numerical stability of barycentric Lagrange interpolation. IMA J. Numer. Anal. **24**(4), 547–556 (2004). <https://doi.org/10.1093/imanum/24.4.547>
- [5] Driscoll, T.A., Hale, N., Trefethen, L.N. (eds.): Chebfun User's Guide. Pafnuty Publications, Oxford (2014). www.chebfun.org.
- [6] Xiang, S., Chen, X., H., W.: Error bounds in chebyshev points. Numer. Math. **116**, 463–491 (2010). <https://doi.org/10.1007/s00211-010-0309-4>
- [7] Shen, J., Tang, T., Wang, L.: Spectral Methods. Springer, Berlin Heidelberg (2011)

- [8] Xiang, S.: On error bounds for orthogonal polynomial expansions and gauss-type quadrature. *SIAM J. Numer. Anal.* **50**, 1240–1263 (2012). <https://doi.org/10.1137/110820841>
- [9] Wang, H., Xiang, S.: On the convergence rates of legendre approximation. *Math. Comput.* **81**(278), 861–877 (2012). <https://doi.org/10.2307/23267976>
- [10] Xie, Z., Wang, L., Zhao, X.: On exponential convergence of gegenbauer interpolation and spectral differentiation. *Math. Comput.* **82**, 1017–1036 (2013). <https://doi.org/10.1090/S0025-5718-2012-02645-7>
- [11] Wang, H., Huybrechs, D., S., V.: Explicit barycentric weights for polynomial interpolation in the roots or extrema of classical orthogonal polynomials. *Math. Comput.* **83**(290), 2893–2914 (2014). <https://doi.org/10.1090/S0025-5718-2014-02821-4>
- [12] Xiang, S.: On interpolation approximation: Convergence rates for polynomial interpolation for functions of limited regularity. *SIAM J. Numer. Anal.* **54**(4), 2083–2113 (2016). <https://doi.org/10.1155/2011/476939>
- [13] Schneider, C., Werner, W.: Some new aspects of rational interpolation. *Math. Comp.* **47**(175), 285–299 (1986). <https://doi.org/10.2307/2008095>
- [14] Berrut, J.-P.: Rational functions for guaranteed and experimentally well-conditioned global interpolation. *Comput. Math. Appl.* **15**(1), 1–16 (1988). [https://doi.org/10.1016/0898-1221\(88\)90067-3](https://doi.org/10.1016/0898-1221(88)90067-3)
- [15] Floater, M.S., Hormann, K.: Barycentric rational interpolation with no poles and high rates of approximation. *Numer. Math.* **107**(2), 315–331 (2007). <https://doi.org/10.1007/s00211-007-0093-y>
- [16] Güttel, S., Klein, G.: Convergence of linear barycentric rational interpolation for analytic functions. *SIAM J. Numer. Anal.* **50**(5), 2560–2580 (2012). <https://doi.org/10.1137/120864787>
- [17] Berrut, J.-P., Klein, G.: Recent advances in linear barycentric rational interpolation. *J. Comput. Appl. Math.* **259**, 95–107 (2014). <https://doi.org/10.1016/j.cam.2013.03.044>
- [18] Tee, T.W., Trefethen, L.N.: A rational spectral collocation method with adaptively transformed Chebyshev grid points. *SIAM J. Sci. Comput.* **28**(5), 1798–1811 (2006). <https://doi.org/10.1137/050641296>
- [19] Hale, N., Tee, T.W.: Conformal maps to multiply slit domains and applications. *SIAM J. Sci. Comput.* **31**(4), 3195–3215 (2009). <https://doi.org/10.1137/080738325>

- [20] Baltensperger, R., Berrut, J.-P., Noël, B.: Exponential convergence of a linear rational interpolant between transformed Chebyshev points. *Math. Comp.* **68**(227), 1109–1120 (1999). <https://doi.org/10.1090/S0025-5718-99-01070-4>
- [21] Nakatsukasa, Y., Sète, O., Trefethen, L.N.: The AAA algorithm for rational approximation. *SIAM J. Sci. Comput.* **40**(3), 1494–1522 (2018). <https://doi.org/10.1137/16M1106122>
- [22] Berrut, J.-P.: The barycentric weights of rational interpolation with prescribed poles. *J. Comput. Appl. Math.* **86**(1), 45–52 (1997). [https://doi.org/10.1016/S0377-0427\(97\)00147-7](https://doi.org/10.1016/S0377-0427(97)00147-7)
- [23] Walsh, J.L.: *Interpolation and Approximation by Rational Functions in the Complex Domain*, 5th edn. American Mathematical Society, Providence (1969)
- [24] Levin, E., Saff, E.B.: Potential theoretic tools in polynomial and rational approximation. In: *Harmonic Analysis and Rational Approximation. Lect. Notes Control Inf. Sci.*, vol. 327, pp. 71–94. Springer, Berlin (2006). https://doi.org/10.1007/11601609_5
- [25] Saff, E.B., Totik, V.: *Logarithmic Potentials with External Fields. Grundlehren der mathematischen Wissenschaften [Fundamental Principles of Mathematical Sciences]*, vol. 316, p. 505. Springer, Berlin (1997). <https://doi.org/10.1007/978-3-662-03329-6>. Appendix B by Thomas Bloom
- [26] Prokhorov, V.A., Saff, E.B.: Rates of best uniform rational approximation of analytic functions by ray sequences of rational functions. *Constr. Approx.* **15**(2), 155–173 (1999). <https://doi.org/10.1007/s003659900103>
- [27] Kythe, P.K.: *Computational Conformal Mapping*, p. 462. Birkhäuser Boston, Inc., Boston (1998). <https://doi.org/10.1007/978-1-4612-2002-2>
- [28] Istace, M.-P., Thiran, J.-P.: On the third and fourth Zolotarev problems in the complex plane. *SIAM J. Numer. Anal.* **32**(1), 249–259 (1995). <https://doi.org/10.1137/0732009>
- [29] Le Bailly, B., Thiran, J.P.: Optimal rational functions for the generalized Zolotarev problem in the complex plane. *SIAM J. Numer. Anal.* **38**(5), 1409–1424 (2000). <https://doi.org/10.1137/S0036142999360688>